Heptagon-Containing Saddle-Shaped Nanographenes: Self-Association and Complexation Studies with Polycyclic Aromatic Hydrocarbons and Fullerenes

Arthur H. G. David[a]
Sandra Míguez-Lago[a]
Carlos M. Cruz[a]
Juan M. Cuerva[a]
Victor Blanco*[a]
Araceli G. Campaña*[a]

[a] Department of Organic Chemistry, Faculty of Sciences, University of Granada. Avda. Fuente Nueva S/N, 18071, Granada, Spain
victorblancos@ugr.es; araceligc@ugr.es

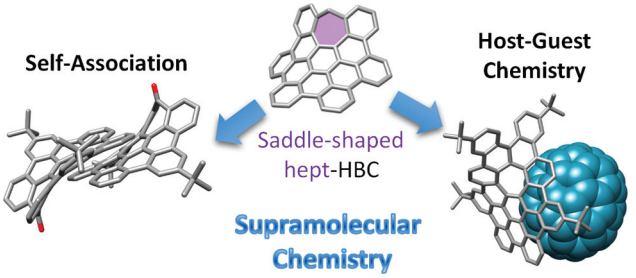

Received: 16.10.2020
Accepted after revision: 14.12.2020
DOI: 10.1055/s-0041-1722848; Art ID: om-20-0035oa

Abstract Supramolecular interactions between molecules of the same or different nature determine to a great extent the degree of their applicability in many fields of science. To this regard, planar polycyclic aromatic hydrocarbons (PAHs) and their nanometric congeners, nanographenes (NGs), as well as positively curved ones, as for instance corannulene, have been extensively explored. However, negatively curved saddle-shaped NGs have remained a curiosity to date within this field. Therefore, here we communicate the first systematic study on the supramolecular behavior of heptagon-containing hexa-*peri*-hexabenzocoronene analogues. Thus, their self-association and host–guest complexation processes with both flat and curved PAHs, and fullerenes have been studied by means of ^{1}H and ^{13}C NMR titrations in solution, identifying C_{70} as one of the guests with the highest association constant among all the ones tested.

Key words nanographenes, contorted aromatics, supramolecular chemistry, host–guest systems, heptacyclic polyarenes, molecular recognition

Introduction

Polycyclic aromatic hydrocarbons (PAHs) have demonstrated to be versatile actors in the field of supramolecular chemistry mainly by virtue of the establishment of π–π and hydrophobic interactions.[1] Their scope ranges from playing the role of host to guest, and even both simultaneously, as in the case of self-association processes. Planar systems are the most broadly explored by far, with examples such as the self-association study of dodecyl-chained hexa-*peri*-hexabenzocoronene (HBC) derivatives reported by Müllen and coworkers.[2] In this case, the association resulted in an upfield shift of the ^{1}H NMR signals upon concentration increase, phenomenon which was subsequently proved to be solvent-dependent,[3] evidencing the influence of the solvophobic effect on the association process. As a result of these supramolecular interactions, diverse applications of the self-association of planar PAHs and nanographenes (NGs) were developed encompassing topics such as the formation of discotic liquid crystals,[4] their implementation in photovoltaic systems,[5,6] supramolecular nanotubes or nanofibers[7,8] displaying relevant optoelectronic,[9–11] sensing[12,13] and spintronic properties,[14] and as organogelators,[15] among others. When it comes to planar PAHs being part of the structure of supramolecular hosts, we find multifarious examples of not only 2D cyclophanes,[16] such as nanohoops encapsulating C_{60} or C_{70},[17–21] but also other kinds of architectures such as metal–organic cages.[22–24] Likewise, planar PAHs such as pyrene or even coronene have been employed as guests for different molecular receptors,[25–30] which is also true for positively curved systems, whose most prominent representative is corannulene.[29,31–33]

The introduction of a curvature within the structure of PAHs and NGs makes them feature higher solubilities on account of the weakening of the π–π stacking. However, this curvature provides, in contrast, access to better host–guest shape complementarities with other curved systems. Corannulene, for instance, binds to C_{60}[34,35] and its incorporation in receptors enables their binding to fullerenes.[36–38] It is also involved in applications derived from its self-association such as liquid crystals,[39] organogelators,[40] and supramolecular polymer formation.[41] Besides, self-aggregation studies of hydrophilic analogues of corannulene functionalized with nucleosides allowed for an uncommon examination in water media.[42]

As opposed to NGs featuring a bowl-shaped positive curvature, literature related to self-association and host–guest behavior of negatively curved saddle-shaped NGs[43,44] containing only heptagonal carbocycles as nonhexagonal

rings remains almost inexistent. Theoretically, Wheeler and coworkers pointed to a better self-association of [7]circulene amongst their smaller and larger [*n*]circulene congeners with $n = 6–10$.[45] Miao and coworkers described an elusive co-crystallization process of a heptacycle-containing NG with C_{60}.[46] In addition to that, in our group we have recently reported the design, synthesis, and use as a selective C_{70} supramolecular receptor of a cyclophane comprising two heptagon-containing HBC analogues (hept-HBCs).[47]

Here we present the first systematic study of the supramolecular behavior of five differently functionalized saddle-shaped hept-HBCs (Figure 1, **1–5**), by examining their self-association as well as their host–guest abilities towards both planar and curved π-systems.

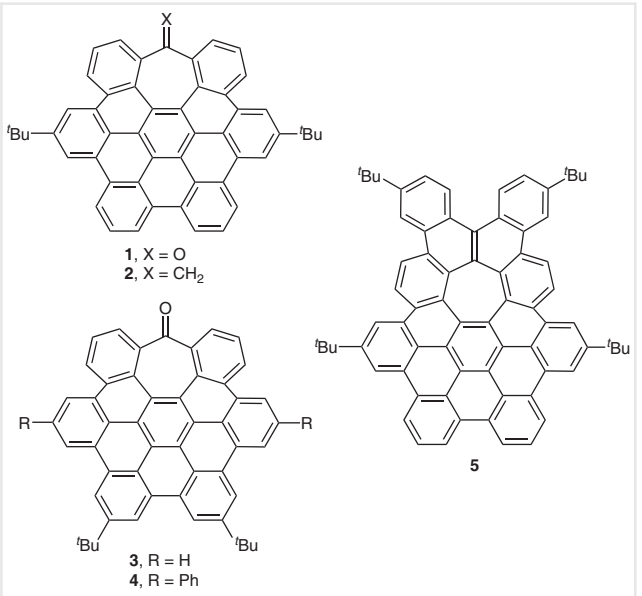

Figure 1 Structures of the heptagon-containing saddle-shaped HBC derivatives **1–5**.

Results and Discussion

Among the collection of hept-HBCs synthesized, the heptagonal carbocycle is either functionalized with carbonyl groups (**1**, **3**, **4**), constituting a tropone unit, a methylene (**2**), or with four additional fused rings extending the π system (**5**). The periphery of the HBCs was decorated either with *tert*-butyl or phenyl groups or hydrogen atoms in proximal (Scheme 1, C_e) or distal positions (Scheme 1, C_h) with respect to the heptacycle. The keystone in the synthesis of all these contorted analogues, developed in our research group, is based on a Co-catalyzed alkyne cyclotrimerization resulting in the simultaneous formation of both the central benzene and the heptacycle rings, followed by a final Scholl cyclodehydrogenation[48] generating the hept-HBC skeleton.[49]

Synthesis of compound **1** was achieved following a procedure described in our group.[49] Subsequent Tebbe

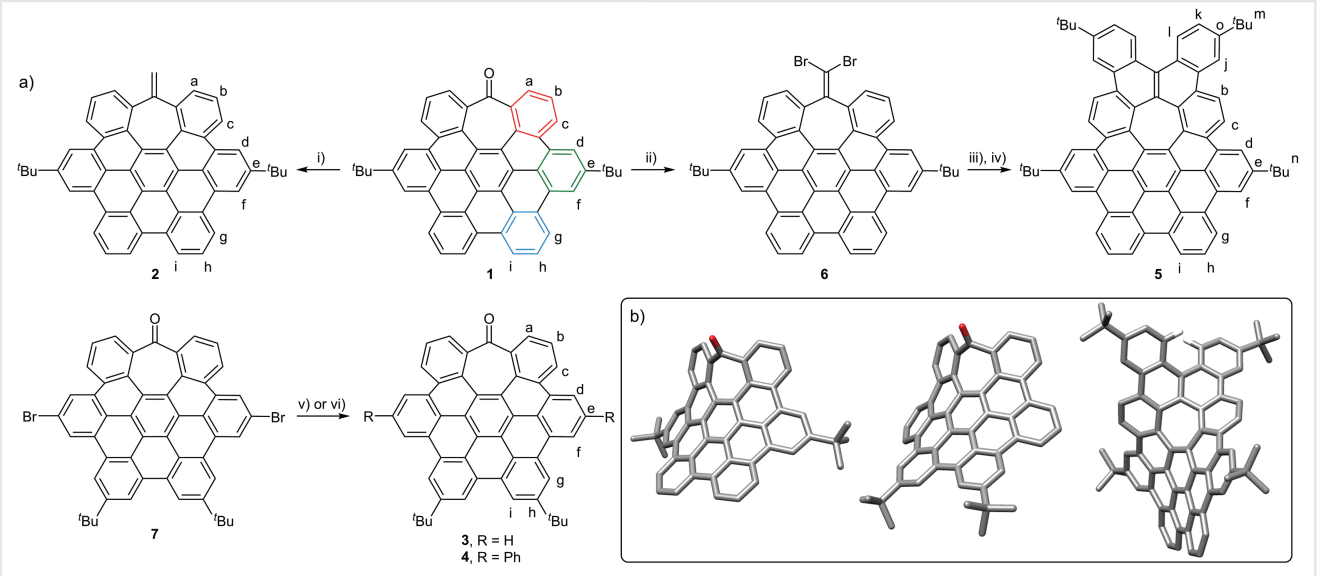

Scheme 1 a) Synthesis of heptagon-containing nanographenes **2–5**. Reagents and conditions: i) Tebbe reagent (0.5 M in toluene), THF, 0 °C to r.t., 2 h, 98%; ii) PPh_3, CBr_4, toluene, reflux, 28 h, 83%; iii) 4-*tert*-butylphenylboronic acid, $Pd(PPh_3)_4$, K_2CO_3, toluene, EtOH/H_2O, 100 °C, 20 h, 84% (see the Supporting Information); iv) $FeCl_3$, 1,2-dichloroethane, CH_3NO_2, 70 °C, 48 h, 96%; v) $Pd(PPh_3)_4$, K_2CO_3, toluene/H_2O/EtOH, reflux, 16 h, 56% (for **3**) ; vi) phenylboronic acid, $Pd(PPh_3)_4$, K_2CO_3, toluene/H_2O/EtOH, reflux, 20 h, 70% (for **4**).[47] b) DFT-optimized structures (ωB97XD/def2SVP in $CHCl_3$) of: **1** (left), **3** (middle), and **5** (right). H atoms have been omitted for clarity.

olefination yielded hept-HBC **2** in 98% yield (Scheme 1, i). Wittig-like reaction over **1** in the presence of CBr_4 and PPh_3 afforded 1,1-dibromoalkene **6** in 83% yield (Scheme 1, ii). Subsequent Suzuki cross-coupling reaction with 4-*tert*-butylphenylboronic acid on intermediate **6** resulted in the dicoupled product in 84% yield (see the Supporting Information), followed by a cyclodehydrogenation reaction using classical $FeCl_3$ conditions providing extended NG **5** in excellent 96% yield (Scheme 1, iii–iv).[50] On the other hand, compounds **3** and **4**[47] were successfully synthesized from precursor **7**,[51] recently reported by our research group. The presence of two bromine atoms in **7** is an appropriate launch pad for further derivatization, which was indeed leveraged in respective reactions under Suzuki cross-coupling conditions without and with phenylboronic acid, giving rise to **3** and **4** in 56% and 70% yields, respectively (Scheme 1, v–vi).

The excellent solubility of compounds **1**–**5** in $CDCl_3$ allowed for their full characterization by means of both 1D and 2D NMR techniques, which enabled the complete assignment of all signals. These data were further supported by HRMS experiments with exact masses and isotopic distributions confirming the proposed structures (for more details, see the Supporting Information).

Derivatives **1**–**5** were also studied using UV-vis spectroscopy. Derivatives **1**–**4** show a similar spectrum with the main absorption features in the 300–400 nm region (Figures S128, S130, S132, and S134 in the Supporting Information). In all cases, the main band has its maximum at around 350–360 nm and exhibits some vibronic structure, less resolved in the case of **1**. Additionally, there is a small band or shoulder centered at 382–391 nm. The position of the substituents does not seem to have much influence on the absorption as the λ_{max} slightly changes when they are attached in different positions (356 nm for **1**, 354 nm for **3**). In addition, the nature of the double bond on the heptagonal ring has a slightly more pronounced effect. Replacing the C = O for a C = C group results in a slight hypsochromic shift of the main absorption band (356 nm for **1**, 351 nm for **3**). On the other hand, the inclusion of aromatic rings as substituents induces an 11 nm bathochromic shift, which can be attributed to some extra delocalization of the π system. Compound **5** has a completely different UV-vis spectrum. It displays a broad absorption between 300 and 450 nm with maxima at 323, 360, and 413 nm and a tail up to ca. 570 nm (Figure S136). This absorption at longer wavelengths is in agreement with the more extended π-surface of this system in comparison with compounds **1**–**4**.

Additionally, hept-HBCs **1**–**5** were investigated theoretically by density functional theory (DFT) computational studies at the ωB97XD/def2SVP or B3LYP/6-31G(d,p) level of calculation in $CHCl_3$, both delivering similar results (for more details see the Supporting Information). Optimized structures revealed, as expected, a saddle-shape curvature, induced by the presence of the heptacycle in NGs **1**–**5**.

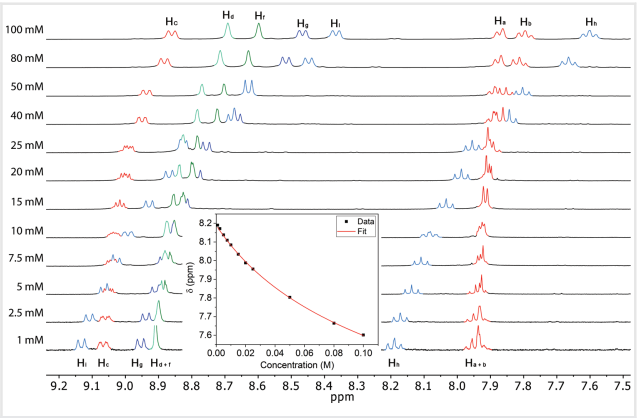

Figure 2 Self-association experiment of nanographene **1**. Aromatic region of the ^{1}H NMR (400 MHz, $CDCl_3$, 298 K) spectra of **1** at different concentrations. Inset: nonlinear least-squares fitting of the changes in the δ (400 MHz, $CDCl_3$, 298 K) of H_h upon concentration change using Eq. 1 (K_d = 3.0 ± 0.2 M^{-1}). Color coding and labels are defined in Scheme 1.

Moreover, additional torsion is shown in the case of **5** owing to steric hindrance between the hydrogen atoms in the cove region. Compound **5** shows, besides, larger dimensions than the rest (16.1 × 11.0 vs. 11.4 × 10.5 Å), which might foster more effective complexations with larger π-systems.

Studies to evaluate the self-association equilibria for species **1**–**5** were conducted via ^{1}H NMR titrations in $CDCl_3$ solution at concentrations ranging from 1 to 100 mM. Upon increasing the concentration of the monomers **1**–**5** during the self-association titrations, an upfield shift is experienced by most of the NG protons (see Figure 2 and Figures S37–S56 in the Supporting Information). A monomer–dimer association model (K_d, Eq. 1)[52] or an indefinite equal *K* self-association model (K_E, Eq. 2)[53] was considered due to the unknown nature of the aggregates formed. The constants were determined by a nonlinear least-squares fitting method through Eq. 1 or Eq. 2. The fitting to these models led to association constants summarized in Table 1, giving rise to values ranging from 1.5 to 24 M^{-1} according to the monomer–dimer model or from 3.1 to 47.3 M^{-1} according to the indefinite one. All values are similar except for **4**, which stands out among their analogues **1**, **2**, **3**, and **5**. This observation matches the augmented π expansion of **4**, provided by the appended phenyl rings in C_e positions, which maximizes the π interactions between the two

Table 1 Self-association constants for NGs **1**–**5**[a]

NG	1	2	3	4	5
K_d (M^{-1})[b]	3.0 ± 0.2	1.5 ± 0.5	6.0 ± 0.6	24 ± 4[d]	6.7 ± 2.0
K_E (M^{-1})[c]	6.2 ± 0.4	3.1 ± 1.1	12.0 ± 1.2	47.3 ± 8	13.3 ± 4.0

[a]Measured by ^{1}H NMR in $CDCl_3$ at 298 K.
[b]Using Eq. 1.
[c]Using Eq. 2.
[d]From Ref. 47.

$$\delta = \Delta\delta \times \left(1 + \frac{1 - \sqrt{8K_dC + 1}}{4K_dC}\right) + \delta_m$$

Equation 1 C denotes the concentration; δ is the observed chemical shift; δ_m is the chemical shift for the monomer; $\Delta\delta$ ($\Delta\delta = \delta_d - \delta_m$) stands for the change in chemical shift from the monomer to the dimer; and K_d represents the association constant for the dimer formation.[52]

$$\delta = \Delta\delta \times \left(1 + \frac{1 - \sqrt{4K_EC + 1}}{2K_EC}\right) + \delta_m$$

Equation 2 C denotes the concentration; δ is the observed chemical shift; δ_m is the chemical shift for the monomer; $\Delta\delta$ ($\Delta\delta = \delta_s - \delta_m$) stands for the change in chemical shift from the monomer to the molecule in the stack; and K_E represents the self-association constant.[53]

monomers. As a result of these low binding constants, the extent of self-association covered in the titrations is far from being complete and this process is relevant at high concentrations, as shown by the calculated α_{agg} values (see the Supporting Information).[54] Only compound **4**, which establishes stronger interactions, shows a significant degree of self-association at low concentrations.

Eq. 1 and Eq. 2 are equivalent, being $K_E = 2K_d$. As a result, distinguishing between association models from the experimental ^{1}H NMR data is not possible[53] and the same fitting was obtained in both cases. Therefore, we cannot unambiguously affirm which of the models describes better the behavior of our system. Nevertheless, an analysis of the expected size of the aggregates formed under this isodesmic model according to Eq. 3 showed that at 0.1 M, the highest concentration used in this work, the number average size of the assemblies is below 2 for all compounds, except for **4**, for which a slightly higher value of ca. 2.7 was calculated (see the Supporting Information, Table S2). In this situation, an equal constant isodesmic model predicts that the species present even at a high concentration are mainly monomers and dimers, except again for compound **4**, in which higher assemblies can be significantly populated.

Analysis of the extension of the shifting of the ^{1}H NMR signals evidences that the position where the ^{t}Bu groups are attached to the hept-HBC core plays a key role in the observed chemical shifts, i.e., when located on the C_h carbon atoms, the major shift was experienced by the H nuclei closer to the tropone moiety ($\Delta\delta_{Hc} = -0.73$ ppm; $\Delta\delta_{Hd} = -0.90$ ppm; $\Delta\delta_{He} = -0.63$ ppm for **3**), whilst when attached to the C_e the influence on the chemical shift is higher for the planar part of the molecules ($\Delta\delta_{Hi} = -0.76$ ppm; $\Delta\delta_{Hh} = -0.59$ ppm; $\Delta\delta_{Hg} = -0.48$ ppm for **1**). However, the modification of the tropone unit by its conversion into the methylidene or the fused diphenylene motifs caused low impact in the resulting self-association process.

$$N = \frac{1 + \sqrt{4K_EC + 1}}{2}$$

Equation 3 N is the number average aggregate size, C denotes the total concentration; K_E represents the self-association constant in the isodesmic model.[54]

Once inquired into the self-association process of saddle-shaped hept-HBCs **1**–**5**, further investigations on their complexation with a selection of guests of different geometry and electronic nature were accomplished. Among the flat guests, we proposed pyrene and benzo[*a*]pyrene as planar nonfunctionalized PAHs, naphthalene diimide (NDI) **8** as a π-acceptor,[55] 1,5-dialkoxynaphthalene **9** as a π-donor, and corannulene, C_{60}, and C_{70} as curved guests (Figure 3). The association constants (K_a) between NGs and PAHs or fullerenes were determined by ^{1}H or ^{13}C NMR titrations in $CDCl_3$ or *o*-DCB-d_4 at r.t. The NMR data were analyzed using a nonlinear least-squares curve fitting procedure performed with the online software *Bindfit*[56] with a 1:1 global fitting model (Nelder–Mead method).[57] Considering the geometry of the hept-HBCs and the guests involved in the binding equilibria, other models such as a 1:2 stoichiometry cannot be ruled out. However, attempts to fit the data to other models proved unsuccessful, as meaningless results were obtained. This is not surprising taking into account the low association observed, which makes binding constants in a 1:2 model very difficult to determine reliably. For this reason a 1:1 model was assumed to obtain an estimation of the binding constants.

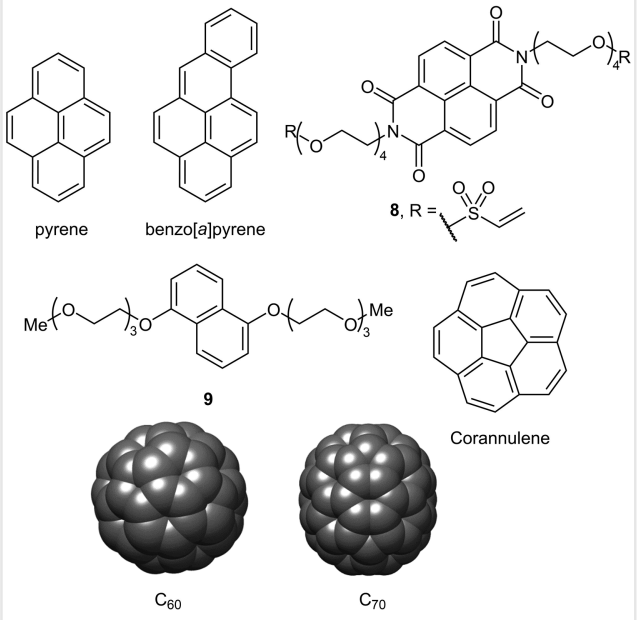

Figure 3 Structures of the guests used in this work.

Table 2 Association constants (K_a, in M^{-1}) between hept-HBCs **1**–**5** and selected guests

Hept-HBC host	Pyrene[a]	Benzo[*a*] pyrene[a]	NDI (**8**)[a]	1,5-Dialkoxy naphthalene (**9**)[a]	Corannulene[a]	C_{60}[b]	C_{70}[b]
1	20.9 ± 0.8	4.07 ± 0.08	17.7 ± 0.3	15.9 ± 0.8	13.5 ± 0.7	12.3 ± 0.2	50.2 ± 2.2
2	8.03 ± 0.11	6.05 ± 0.06	21.8 ± 0.7	7.96 ± 0.34	13.4 ± 0.7	15.8 ± 0.2	35.3 ± 1.3
3	<0.01	3.67 ± 0.06	9.40 ± 0.13	36.6 ± 2.6	8.40 ± 0.53	8.13 ± 0.07	28.3 ± 0.7
4	<0.01	4.73 ± 0.12	7.26 ± 0.11	18.4 ± 1.2	<0.01	20.0 ± 0.1[c]	3.75 ± 0.02[c]
5	8.04 ± 0.18	6.48 ± 0.13	17.7 ± 0.2	65.7 ± 2.1	10.9 ± 0.5	18.5 ± 0.3	53.1 ± 2.4

[a]Measured by ^{1}H NMR in $CDCl_3$.
[b]Measured by ^{13}C NMR in *o*-DCB-d_4.
[c]From Ref. 47.

When we glance at K_a results,[58] summarized in Table 2, we conclude that, in general, the best results for the planar guests were found for the complexes assembled with both the electron acceptor and donor **8** and **9**, respectively. On the other hand, the lack of complexation between hosts **3** and **4** and pyrene as a guest, both bearing ^{t}Bu groups in C_h positions, hints at a disfavored binding due to this structural feature. Nevertheless, recognition of benzo[*a*]pyrene was of the same magnitude for all hosts, while again for NDI **8**, the binding is better for derivatives **1** and **2**, with ^{t}Bu groups in the C_e position. Besides, dialkoxynaphthalene **9** reached the maximum K_a value with guest **5**, and, overall, these NGs, except for host **2**, are more prone to complex electron-rich PAHs.

Furthermore, from the variation of the ^{1}H NMR signals during the titrations, it is inferred that the interactions between hept-HBCs **1**–**5** with pyrene, benzo[*a*]pyrene, and NDI **8** (Figure 4 and Figures S57–S60, S67–S72, S77–S82, S87–S92, S97–S102 in the Supporting Information) take place in the more planar part of the hosts. In the case of electron-rich guest **9**, the changes on chemical shift are minimal (up to |0.02| ppm), which hampers the clear correlation between shift and host–guest interaction location (see Figures S63, S64, S73, S74, S83, S84, S93, S94, S103, and S104 in the Supporting Information).

When we evaluate the interaction with the first curved guest, corannulene, similar K_a values were found for all guests aside from **4**, with which no recognition was found (see Figures S65, S66, S75, S76, S85, S86, S95, S96, S105, and S106 in the Supporting Information). Finally, among the binding abilities of hept-HBCs **1**–**5** with fullerenes C_{60} and C_{70} (see Figures S107–S122 in the Supporting Information), it is worth mentioning that a K_a of ca. 53 M^{-1} is observed between π-extended **5** and C_{70}, and, as a trend, there is a clear preference for C_{70} over C_{60}, except for host **4**, conceivably due to the presence of the phenyl rings on position C_e. Last, a comparison between the affinity of hosts **1** and **3** towards C_{70} points to a preference for the compound with the ^{t}Bu groups closer to the troponic carbonyl group of the molecule.

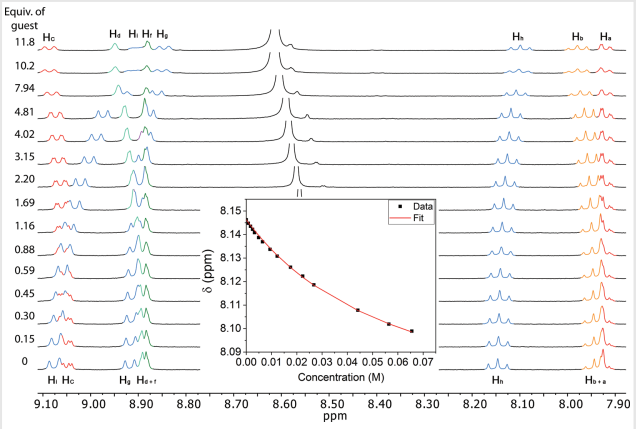

Figure 4 Aromatic region of the ^{1}H NMR (400 MHz, $CDCl_3$, 298 K) spectra for the titration of **1** with **8** (0–11.8 equiv). Inset: fitted binding isotherm using a 1:1 association model (K_a = 17.7 ± 0.3 M^{-1}) showing the change in the chemical shift for H_h. Color coding and labels are defined in Scheme 1.

Conclusions

Five saddle-shaped hept-HBCs **1**–**5** were synthesized and fully characterized. Moreover, their self-association properties were proven, finding the position and the nature of the peripheral groups to play an important role in the aggregation of these compounds. On the contrary, the enhancement of the distortion of these contorted HBC derivatives or the modification of the tropone unit revealed to have little effect on the self-association properties. Besides, the complexation ability of contorted NGs **1**–**5** towards PAHs and fullerenes was demonstrated, with its maximum exponent in the recognition between π-extended host **5** and electron donor guest **9** (K_a = 66 M^{-1}) and fullerene C_{70} (K_a = 53 M^{-1}). Thus, this study points at a promising future of the supramolecular chemistry of negatively curved hept-HBCs, as confirmed by their self-association and the sensing of PAHs and fullerenes.

Experimental Section

Experimental Details

Unless otherwise noted, commercially available reagents, solvents, and anhydrous solvents were used as purchased without further purification. Anhydrous THF was freshly distilled over Na/benzophenone. $Pd(PPh_3)_4$,[59] and compounds **1**,[49] **4**,[47] **7**,[51] and **8**[55] were prepared according to literature procedures.

TLC was performed on Merck Silica gel 60 F_{254} aluminum sheets. The TLC plates were stained with potassium permanganate (1% w/v in water) or observed under UV light when applicable. Flash column chromatography was performed with Silica gel 60 (VWR, 40–63 µm).

^1H and ^{13}C NMR spectra were recorded at room temperature on a Varian Direct Drive (400 or 500 MHz), Bruker Avance III HD NanoBay (400 MHz), or Bruker Avance Neo (400 or 500 MHz) spectrometers at a constant temperature of 298 K. Chemical shifts are given in ppm and referenced to the signal of the residual protiated solvent (^1H: $\delta = 7.26$ for $CDCl_3$) or the ^{13}C signal of the solvents (^{13}C: $\delta = 77.16$ for $CDCl_3$ or $\delta = 132.39$ for *o*-DCB-d_4) or to the signal of the residual TMS (^1H: $\delta = 0.00$). Coupling constant (J) values are given in Hz. Abbreviations indicating multiplicity are as follow: m = multiplet, p = quintet, q = quartet, t = triplet, d = doublet, dd = doublet of doublets, td = triplet of doublets, s = singlet, br = broad. Signals were assigned by means of 2D NMR spectroscopy (COSY, heteronuclear single-quantum correlation spectroscopy, heteronuclear multiple bond correlation spectroscopy).

Electrospray (ESI) HRMS spectra were recorded on a Waters Xevo G2-XS QTOF or on a Bruker Maxis II spectrometer. MALDI mass spectra were recorded on a Bruker Ultraflex III mass spectrometer. IR spectra were recorded with a Perkin–Elmer Spectrum Two FTIR ATR spectrometer.

Self-Association Studies

Solutions of NGs at different concentrations (1–100 mM) were prepared in $CDCl_3$ using volumetric flasks and volumetric pipettes. The ^1H NMR spectra at each concentration were recorded.

PAH-Binding Studies

For the titrations with PAHs, a solution of the corresponding hept-HBC derivative was prepared in $CDCl_3$ using a micropipette. Then, the solution of the corresponding PAH was prepared in another vial using the solution of the NG as a solvent in order to maintain a constant concentration of hept-HBC during the titration experiment. The addition of the solution of the PAH to the NG solution (450 µL) was carried out with Hamilton® syringes typically using the following order: 4 × 3, 2 × 6, 2 × 12, 3 × 24, 3 × 120 µL. After each addition, the solution was shaken for 30 seconds and the ^1H NMR spectrum was recorded.

Fullerene-Binding Studies

For the titrations with fullerene, a solution of the corresponding fullerene was prepared in *o*-DCB-d_4 using a micropipette. Then, the solution of the corresponding hept-HBC was prepared in another vial using the solution of the fullerene as a solvent in order to maintain a constant concentration of fullerene during the titration experiment. The addition of the solution of the NG to the fullerene solution (500 µL) was carried out with Hamilton® syringes typically using the following order: 8 × 16, 2 × 32, 4 × 64 µL (for C_{60}) and 1 × 16, 4 × 32, 4 × 64, 1 × 90 µL (for C_{70}). After each addition, the solution was shaken for 30 seconds and the ^{13}C NMR spectrum was recorded.

Computational Methods

DFT theoretical calculations were performed at the B3LYP/6-31G(d,p) or ωB97XD/def2SVP levels for the five heptagon-containing NG analogues using the Gaussian 09 software package.[60] Chloroform was used as a solvent, applying the polarizable continuum model with the integral equation formalism (IEFPCM) implemented in Gaussian 09. Frequency calculations were performed to confirm the optimized structures corresponded to energy minima.

Procedures

Compound 2

To a degassed solution of **1** (50 mg, 0.075 mmol) in freshly distilled anhydrous THF (10 mL), cooled in a water-ice bath, was added the Tebbe reagent (0.5 M in toluene, 0.20 mL, 0.10 mmol). The solution was stirred for 5 min at 0–4 °C and 15 min at r.t. The round-bottom flask was again immersed in a water-ice bath and Tebbe reagent (0.5 M in toluene, 0.20 mL, 0.10 mmol) was added. The solution was stirred for 5 min at 0–4 °C and 15 min at r.t. This operation was repeated another time and the solution was stirred for 1 h at r.t. Subsequently, $NaOH_{(aq)}$ (1 M; 10 mL) was added to quench the reaction. The resulting mixture was diluted with H_2O (20 mL) and extracted with CH_2Cl_2 (3 × 30 mL). The

combined organic phases were dried over Na_2SO_4 and the solvent was evaporated under reduced pressure. The crude material was purified by column chromatography (SiO_2, CH_2Cl_2/hexane 10:90 then 20:80) to yield **2** (49 mg, 98%) as a yellow solid.

^{1}H NMR (500 MHz, $CDCl_3$): δ = 8.88–8.84 (m, 6 H, H_{c+d+i}), 8.79 (m, 4 H, H_{f+g}), 7.95 (t, J = 7.7 Hz, 2 H, H_h), 7.87 (t, J = 7.6 Hz, 2 H, H_b), 7.68 (d, J = 6.4 Hz, 2 H, H_a), 5.08 (s, 2 H, H_{CH2}), 1.64 (s, 18 H, H^t_{Bu}).

^{13}C NMR (126 MHz, $CDCl_3$): δ = 152.92, 149.80, 143.95, 131.45, 130.57, 130.00, 129.77, 128.96, 128.64, 127.91, 126.97, 125.85, 124.90, 124.28, 123.50, 123.12, 122.53, 121.92, 121.53, 120.70, 120.40, 118.18, 115.28, 35.67, 31.95.

IR (neat): 2956, 1613, 1588, 1462, 1368, 1256, 1078 cm^{-1}.

HRMS (ESI$^+$): m/z $[M + Na]^+$ calcd for $C_{52}H_{36}Na$: 683.2715; found: 683.2737.

Compound 6

To a degassed solution of **1** (346 mg, 0.522 mmol) in anhydrous toluene (20 mL) were added PPh_3 (1.30 g, 4.95 mmol) and CBr_4 (865 mg, 2.61 mmol). The suspension was refluxed for 28 h. The solvent was removed under reduced pressure and the crude material was purified by column chromatography (SiO_2, CH_2Cl_2/hexane 20:80) to afford **6** (355 mg, 83%) as a yellow solid.

^{1}H NMR (500 MHz, $CDCl_3$): δ = 8.91 (m, 4 H), 8.81 (m, 6 H), 7.94 (m, 4 H), 7.77 (d, J = 7.2 Hz, 2 H), 1.65 (s, 18 H).

^{13}C NMR (126 MHz, $CDCl_3$): δ = 150.01, 147.31, 140.96, 132.14, 130.58, 130.04, 130.02, 128.30, 128.21, 127.80, 127.12, 124.81, 124.63, 123.97, 123.63, 123.09, 122.50, 122.05, 121.67, 120.87, 120.76, 118.11, 90.43, 35.74, 31.97.

IR (neat): 2957, 1675, 1612, 1588, 1463, 1393, 1078, 811 cm^{-1}.

HRMS (MALDI$^+$): m/z $[M]^+$ calcd for $C_{52}H_{34}Br$: 816.1022; found: 816.1015.

Compound 5

A degassed solution of **S1** (see the Supporting Information) (128 mg, 0.138 mmol) in 1,2-dichloroethane (180 mL) was split in six different 50 mL round-bottom flasks. These solutions were heated to 70 °C and subsequently, in each flask was added a degassed solution of $FeCl_3$ (75 mg) in dry CH_3NO_2 (500 µL) portionwise. These solutions were further stirred for 48 h at 70 °C. The six resulting mixtures were combined, diluted with CH_2Cl_2 (100 mL) and washed with brine (150 mL). The organic layer was then dried over Na_2SO_4 and the solvent was evaporated under vacuum. The crude material was purified by column chromatography (SiO_2, CH_2Cl_2/hexane 20:80) to give **5** (124 mg, 96%) as an orange solid.

^{1}H NMR (500 MHz, $CDCl_3$): δ = 8.94 (d, J = 1.8 Hz, 2 H, H_f), 8.89 (d, J = 7.9 Hz, 2 H, H_i), 8.75 (d, J = 8.0 Hz, 2 H, H_g), 8.42 (d, J = 1.8 Hz, 2 H, H_d), 8.37 (d, J = 2.0 Hz, 2 H, H_j), 8.30 (d, J = 8.6 Hz, 2 H, H_c), 8.20 (m, 4 H, H_{b+k}), 7.97 (t, J = 7.7 Hz, 2 H, H_h), 7.61 (dd, J = 8.8, 2.0 Hz, 2 H, H_l), 1.66 (s, 18 H, H_n), 1.48 (s, 18 H, H_m).

^{13}C NMR (126 MHz, $CDCl_3$): δ = 149.98, 149.82, 134.53, 133.93, 131.01, 130.76, 130.49, 130.03, 130.00, 129.54, 129.53, 128.82, 128.25, 127.03, 126.68, 126.43, 125.23, 124.74, 124.35, 124.08, 122.48, 122.38, 122.13, 121.38, 121.36, 119.31, 119.16, 118.17, 116.99, 35.73, 35.27, 32.02, 31.62.

IR (neat): 3390 (br), 2957, 2922, 2852, 1612, 1589, 1462, 1363, 1262, 1093, 1024 cm^{-1}.

HRMS (MALDI$^+$): m/z $[M]^+$ calcd for $C_{72}H_{56}$: 920.4377; found: 920.4383.

Compound 3

To a degassed solution of **7** (91 mg, 0.11 mmol) in toluene (6 mL) were added $Pd(PPh_3)_4$ (38 mg, 0.033 mmol), K_2CO_3 (306 mg, 2.22 mmol), and a degassed mixture of EtOH/H_2O (3:1, 4 mL). The mixture was refluxed for 16 h. Subsequently, $HCl_{(aq)}$ (5%, 30 mL) was added and the resulting mixture was extracted with CH_2Cl_2 (3 × 50 mL). The combined organic phases were dried over Na_2SO_4 and the solvent was removed under reduced pressure. The crude material was purified by column chromatography (SiO_2, CH_2Cl_2/hexane 60:40) to afford **3** (41 mg, 56%) as a yellow solid.

^{1}H NMR (500 MHz, $CDCl_3$): δ = 9.13 (d, J = 1.7 Hz, 2 H, H_i), 8.76 (d, J = 1.7 Hz, 2 H, H_g), 8.54 (t, J = 4.9 Hz, 2 H, H_c), 8.49 (d, J = 7.6 Hz, 2 H, H_f), 8.23 (d, J = 7.8 Hz, 2 H, H_d), 7.66 (m, 6 H, H_{a+b+e}), 1.77 (s, 18 H, H^t_{Bu}).

^{13}C NMR (126 MHz, $CDCl_3$): δ = 202.60, 149.97, 142.07, 130.89, 129.90, 129.81, 128.15, 127.24, 127.03, 126.82, 126.54, 124.76, 124.16, 123.87, 123.03, 122.71, 122.59, 120.56, 120.48, 119.45, 118.62, 35.84, 32.11.

IR (neat): ν = 2955, 2924, 2862, 1671, 1609, 1588, 1392, 1362, 1336, 1255 cm^{-1}.

HRMS (ESI$^+$): m/z $[M + Na]^+$ calcd for $C_{51}H_{34}ONa$: 685.2507; found: 685.2530; m/z $[M + H]^+$ calcd for $C_{51}H_{35}O$: 663.2688; found: 663.2697.

Funding Information

We acknowledge FEDER/Junta de Andalucía (A-FQM-339-UGR18, Programa Operativo FEDER 2014-2020, Consejería de Economía y Conocimiento), the European Research Council (ERC) under the European Union's Horizon 2020 research and innovation program (ERC-2015-STG-677023), and Ministerio de Ciencia, Innovación y Universidades (MICIU/FEDER/AEI, Spain; PGC2018-101181-B-I00) for financial support.

Acknowledgment

The authors thank the Centro de Servicios de Informática y Redes de Comunicaciones (CSIRC), Universidad de Granada, for providing the computing time.

Supporting Information

Supporting Information for this article is available online at https://doi.org/10.1055/s-0041-1722848.

References

(1) Steed, J. W.; Atwood, J. L. Supramolecular Chemistry, 2nd Edition. John Wiley & Sons: Chichester, **2009**.
(2) Wu, J.; Fechtenkötter, A.; Gauss, J.; Watson, M. D.; Kastler, M.; Fechtenkötter, C.; Wagner, M.; Müllen, K. *J. Am. Chem. Soc.* **2004**, *126*, 11311.
(3) Kastler, M.; Pisula, W.; Wasserfallen, D.; Pakula, T.; Müllen, K. *J. Am. Chem. Soc.* **2005**, *127*, 4286.
(4) Herwig, P.; Kayser, C. W.; Müllen, K.; Spiess, H. W. *Adv. Mater.* **1996**, *8*, 510.
(5) Schmidt-Mende, L.; Fechtenkötter, A.; Müllen, K.; Moons, E.; Friend, R. H.; MacKenzie, J. D. *Science* **2001**, *293*, 1119.
(6) Wong, W. W. H.; Subbiah, J.; Puniredd, S. R.; Purushothaman, B.; Pisula, W.; Kirby, N.; Müllen, K.; Jones, D. J.; Holmes, A. B. *J. Mater. Chem.* **2012**, *22*, 21131.
(7) Hill, J. P.; Jin, W.; Kosaka, A.; Fukushima, T.; Ichihara, H.; Shimomura, T.; Ito, K.; Hashizume, T.; Ishii, N.; Aida, T. *Science* **2004**, *304*, 1481.
(8) Kulkarni, C.; Munirathinam, R.; George, S. J. *Chem. Eur. J.* **2013**, *19*, 11270.
(9) Yamamoto, Y.; Fukushima, T.; Jin, W.; Kosaka, A.; Hara, T.; Nakamura, T.; Saeki, A.; Seki, S.; Tagawa, S.; Aida, T. *Adv. Mater.* **2006**, *18*, 1297.
(10) Yamamoto, Y.; Fukushima, T.; Suna, Y.; Ishii, N.; Saeki, A.; Seki, S.; Tagawa, S.; Taniguchi, M.; Kawai, T.; Aida, T. *Science* **2006**, *314*, 1761.
(11) Treier, M.; Liscio, A.; Mativetsky, J. M.; Kastler, M.; Müllen, K.; Palermo, V.; Samorì, P. *Nanoscale* **2012**, *4*, 1677.
(12) Mogera, U.; Gedda, M.; George, S. J.; Kulkarni, G. U. *ACS Appl. Mater. Interfaces* **2017**, *9*, 32065.
(13) Mogera, U.; Sagade, A. A.; George, S. J.; Kulkarni, G. U. *Sci. Rep.* **2014**, *4*, 4103.
(14) Kulkarni, C.; Mondal, A. K.; Das, T. K.; Grinbom, G.; Tassinari, F.; Mabesoone, M. F. J.; Meijer, E. W.; Naaman, R. *Adv. Mater.* **2020**, *32*, 1904965.
(15) Ito, S.; Herwig, P. T.; Böhme, T.; Rabe, J. P.; Rettig, W.; Müllen, K. *J. Am. Chem. Soc.* **2000**, *122*, 7698.
(16) Li, G.; Matsuno, T.; Han, Y.; Phan, H.; Wu, S.; Jiang, Q.; Zou, Y.; Isobe, H.; Wu, J. *Angew. Chem. Int. Ed.* **2020**, *59*, 9727.
(17) Lu, D.; Zhuang, G.; Wu, H.; Wang, S.; Yang, S.; Du, P. *Angew. Chem. Int. Ed.* **2017**, *56*, 158.
(18) Cui, S.; Zhuang, G.; Lu, D.; Huang, Q.; Jia, H.; Wang, Y.; Yang, S.; Du, P. *Angew. Chem. Int. Ed.* **2018**, *57*, 9330.
(19) Huang, Q.; Zhuang, G.; Jia, H.; Qian, M.; Cui, S.; Yang, S.; Du, P. *Angew. Chem. Int. Ed.* **2019**, *58*, 6244.
(20) Lu, D.; Huang, Q.; Wang, S.; Wang, J.; Huang, P.; Du, P. *Front. Chem.* **2019**, *7*, 668.
(21) Xu, Y.; von Delius, M. *Angew. Chem. Int. Ed.* **2020**, *59*, 559.
(22) Suzuki, K.; Takao, K.; Sato, S.; Fujita, M. *J. Am. Chem. Soc.* **2010**, *132*, 2544.
(23) Ronson, T. K.; League, A. B.; Gagliardi, L.; Cramer, C. J.; Nitschke, J. R. *J. Am. Chem. Soc.* **2014**, *136*, 15615.
(24) Ronson, T. K.; Meng, W.; Nitschke, J. R. *J. Am. Chem. Soc.* **2017**, *139*, 9698.
(25) Yamashina, M.; Tanaka, Y.; Lavendomme, R.; Ronson, T. K.; Pittelkow, M.; Nitschke, J. R. *Nature* **2019**, *574*, 511.
(26) Dale, E. J.; Vermeulen, N. A.; Juríček, M.; Barnes, J. C.; Young, R. M.; Wasielewski, M. R.; Stoddart, J. F. *Acc. Chem. Res.* **2016**, *49*, 262.
(27) Liu, X. T.; Wang, K.; Chang, Z.; Zhang, Y. H.; Xu, J.; Zhao, Y. S.; Bu, X. H. *Angew. Chem. Int. Ed.* **2019**, *58*, 13890.
(28) Lozano, D.; Álvarez-Yebra, R.; López-Coll, R.; Lledó, A. *Chem. Sci.* **2019**, *10*, 10351.
(29) Ibáñez, S.; Peris, E. *Angew. Chem. Int. Ed.* **2020**, *59*, 6860.
(30) Blanco, V.; García, M. D.; Terenzi, A.; Pía, E.; Fernández-Mato, A.; Peinador, C.; Quintela, J. M. *Chem. Eur. J.* **2010**, *16*, 12373.
(31) Schmidt, B. M.; Osuga, T.; Sawada, T.; Hoshino, M.; Fujita, M. *Angew. Chem. Int. Ed.* **2016**, *55*, 1561.
(32) Joshi, H.; Sreejith, S.; Dey, R.; Stuparu, M. C. *RSC Adv.* **2016**, *6*, 110001.
(33) Fan, Q. J.; Lin, Y. J.; Hahn, F. E.; Jin, G. X. *Dalton Trans.* **2018**, *47*, 2240.
(34) Mizyed, S.; Georghiou, P. E.; Bancu, M.; Cuadra, B.; Rai, A. K.; Cheng, P.; Scott, L. T. *J. Am. Chem. Soc.* **2001**, *123*, 12770.
(35) Georghiou, P. E.; Tran, A. H.; Mizyed, S.; Bancu, M.; Scott, L. T. *J. Org. Chem.* **2005**, *70*, 6158.
(36) Sygula, A.; Fronczek, F. R.; Sygula, R.; Rabideau, P. W.; Olmstead, M. M. *J. Am. Chem. Soc.* **2007**, *129*, 3842.
(37) Yanney, M.; Sygula, A. *Tetrahedron Lett.* **2013**, *54*, 2604.
(38) Barbero, H.; Ferrero, S.; Álvarez-Miguel, L.; Gómez-Iglesias, P.; Miguel, D.; Álvarez, C. M. *Chem. Commun.* **2016**, *52*, 12964.
(39) Miyajima, D.; Tashiro, K.; Araoka, F.; Takezoe, H.; Kim, J.; Kato, K.; Takata, M.; Aida, T. *J. Am. Chem. Soc.* **2009**, *131*, 44.
(40) Mattarella, M.; Haberl, J. M.; Ruokolainen, J.; Landau, E. M.; Mezzenga, R.; Siegel, J. S. *Chem. Commun.* **2013**, *49*, 7204.
(41) Kang, J.; Miyajima, D.; Mori, T.; Inoue, Y.; Itoh, Y.; Aida, T. *Science* **2015**, *347*, 646.
(42) Mattarella, M.; Berstis, L.; Baldridge, K. K.; Siegel, J. S. *Bioconjugate Chem.* **2014**, *25*, 115.
(43) Márquez, I. R.; Castro-Fernández, S.; Millán, A.; Campaña, A. G. *Chem. Commun.* **2018**, *54*, 6705.
(44) Pun, S. H.; Miao, Q. *Acc. Chem. Res.* **2018**, *51*, 1630.
(45) Guan, Y.; Jones, M. L.; Miller, A. E.; Wheeler, S. E. *Phys. Chem. Chem. Phys.* **2017**, *19*, 18186.
(46) Gu, X.; Li, H.; Shan, B.; Liu, Z.; Miao, Q. *Org. Lett.* **2017**, *19*, 2246.
(47) Jiménez, V. G.; David, A. H. G.; Cuerva, J. M.; Blanco, V.; Campaña, A. G. *Angew. Chem. Int. Ed.* **2020**, *59*, 15124.
(48) Zhai, L.; Shukla, R.; Rathore, R. *Org. Lett.* **2009**, *11*, 3474.
(49) Márquez, I. R.; Fuentes, N.; Cruz, C. M.; Puente-Muñoz, V.; Sotorrios, L.; Marcos, M. L.; Choquesillo-Lazarte, D.; Biel, B.; Crovetto, L.; Gómez-Bengoa, E.; González, M. T.; Martin, R.; Cuerva, J. M.; Campaña, A. G. *Chem. Sci.* **2017**, *8*, 1068.
(50) Cheung, K. Y.; Xu, X.; Miao, Q. *J. Am. Chem. Soc.* **2015**, *137*, 3910.
(51) Castro-Fernández, S.; Cruz, C. M.; Mariz, I. F. A.; Márquez, I. R.; Jiménez, V. G.; Palomino-Ruiz, L.; Cuerva, J. M.; Maçôas, E.; Campaña, A. G. *Angew. Chem. Int. Ed.* **2020**, *59*, 7139.
(52) Chu, M.; Scioneaux, A. N.; Hartley, C. S. *J. Org. Chem.* **2014**, *79*, 9009.
(53) Martin, R. B. *Chem. Rev.* **1996**, *96*, 3043.

(54) Chen, Z.; Lohr, A.; Saha-Möller, C. R.; Würthner, F. *Chem. Soc. Rev.* **2009**, *38*, 564.
(55) David, A. H. G.; García-Cerezo, P.; Campaña, A. G.; Santoyo-González, F.; Blanco, V. *Chem. Eur. J.* **2019**, *25*, 6170.
(56) http://supramolecular.org/ (January 4, 2021).
(57) Thordarson, P. *Chem. Soc. Rev.* **2011**, *40*, 1305.
(58) The K_a values presented have not been corrected to take into account the influence of the self-association of the hept-HBC derivatives or the guests benzo[*a*]pyrene or **8**, which also have some tendency to self-associate. These processes can be included in the binding in some cases assuming the simpler monomer–dimer model to study the self-association and considering that the self-assembled species (i.e., dimers) can also form heteroassemblies as they have two π surfaces available. However, a maximum variation of ca. 10% was observed in the values of the binding constants, so this effect can be omitted in a reasonable approximation.
(59) Coulson, D. R.; Satek, L. C.; Grim, S. O. *Inorg. Synth.* **1972**, *13*, 121.
(60) Frisch, M. J.; Trucks, G. W.; Schlegel, H. B.; Scuseria, G. E.; Robb, M. A.; Cheeseman, J. R.; Scalmani, G.; Barone, V.; Mennucci, B.; Petersson, G. A.; Nakatsuji, H.; Caricato, M.; Li, X.; Hratchian, H. P.; Izmaylov, A. F.; Bloino, J.; Zheng, G.; Sonnenberg, J. L.; Hada, M.; Ehara, M.; Toyota, K.; Fukuda, R.; Hasegawa, J.; Ishida, M.; Nakajima, T.; Honda, Y.; Kitao, O.; Nakai, H.; Vreven, T.; Montgomery, J. A. Jr; Peralta, J. E.; Ogliaro, F.; Bearpark, M.; Heyd, J. J.; Brothers, E.; Kudin, K. N.; Staroverov, V. N.; Keith, T.; Kobayashi, R.; Normand, J.; Raghavachari, K.; Rendell, A.; Burant, J. C.; Iyengar, S. S.; Tomasi, J.; Cossi, M.; Rega, N.; Millam, J. M.; Klene, M.; Knox, J. E.; Cross, J. B.; Bakken, V.; Adamo, C.; Jaramillo, J.; Gomperts, R.; Stratmann, R. E.; Yazyev, O.; Austin, A. J.; Cammi, R.; Pomelli, C.; Ochterski, J. W.; Martin, R. L.; Morokuma, K.; Zakrzewski, V. G.; Voth, G. A.; Salvador, P.; Dannenberg, J. J.; Dapprich, S.; Daniels, A. D.; Farkas, O.; Foresman, J. B.; Ortiz, J. V.; Cioslowski, J.; Fox, D. J. Gaussian 09, Revision B.01. Gaussian, Inc.: Wallingford, CT, **2010**.